Materials and Design 43 (2013) 373–383

Contents lists available at SciVerse ScienceDirect

Materials and Design

journal homepage: www.elsevier.com/locate/matdes

Tensile and fatigue properties of fiber laser welded high strength low alloy and DP980 dual-phase steel joints

W. Xu [a], D. Westerbaan [b], S.S. Nayak [b], D.L. Chen [a,*], F. Goodwin [c], Y. Zhou [b]

[a] Department of Mechanical and Industrial Engineering, Ryerson University, 350 Victoria Street, Toronto, Ontario M5B 2K3, Canada
[b] Department of Mechanical and Mechatronics Engineering, University of Waterloo, 200 University Avenue West, Waterloo, Ontario N2L 3G1, Canada
[c] International Zinc Association, Durham, NC 27713, USA

ARTICLE INFO

Article history:
Received 2 June 2012
Accepted 8 July 2012
Available online 16 July 2012

Keywords:
Fiber laser welding
High strength low alloy steel
Dual-phase steel
Microstructure
Fatigue

ABSTRACT

The study was aimed at evaluating the microstructure and mechanical properties of high-speed fiber laser welded high strength low alloy (HSLA) and DP980 dual-phase steel joints with varying weld geometries. Fusion zone (FZ) consisted of martensitic structure, and heat-affected zone (HAZ) contained newly-formed martensite in both steels and partially tempered martensite in DP980. While HAZ-softening was present in DP980, it was absent in HSLA. A distinctive "suspension bridge"-like hardness profile with the FZ hardness as a "pylon" appeared in the fiber laser welded joints. Both HSLA and DP980 joints showed a superior tensile strength, with a joint efficiency of 94–96% and 96–97%, respectively, despite a reduced elongation in DP980 joints. Fatigue strength was higher in DP980 joints than in HSLA joints at higher stress amplitudes, but had no obvious difference at lower stress amplitudes. DP980 multiple linear welds exhibited a larger scatter and lower fatigue strength. Fatigue failure of HSLA joints occurred in the base metal at a stress amplitude above 250 MPa, and at weld concavity at a lower stress amplitude below 250 MPa. Fatigue crack in DP980 joints initiated predominantly from the weld concavity at both high and low levels of stress amplitudes.

1. Introduction

The demand of environment-friendly vehicles that have better fuel economy and lower CO_2 emissions compels automakers to apply advanced technology and new materials in vehicle manufacturing [1–4]. During manufacturing of automotive components, welding and joining are unavoidable. Laser welding is an enabling technology which is fast and precise in joining a wide variety of materials with varying thicknesses and types [5,6]. A new generation of fiber lasers has been developed for industrial applications and has multiple advantages, including high power with small beam divergence, flexible beam delivery, low maintenance costs, high efficiency, and compact size [7,8].

A lot of studies on laser welding of HSLA, DP980, and other steels have been reported in the literature [9–12]. For example, Saunders and Wagone [9] conducted a study on Nd:YAG and CO_2 laser welding of the aluminum-killed drawing quality (AKDQ) steel and HSLA steel sheets in which they concluded that the intrinsic ductility of AKDQ and HSLA steel reduced after laser welding. In another study, Sreenivasan et al. [10] investigated the mechanical properties and performance of DP980 steel tailor welded blanks manufactured using Nd:YAG and diode laser welding (DLW). Formability and uniaxial tensile strength of DP980 welded blanks significantly reduced due to the occurrence of heat affected zone (HAZ)-softening, i.e., the hardness at outer HAZ being significantly below that of the base material caused by tempering of martensite. Similar effect of HAZ-softening on the formability was observed by Xia et al. [11] in their comparative study of HSLA and DP980 steel joints prepared using DLW. The study suggested a lower formability of DP980 diode laser welded blanks compared to the base metal (BM), which could be improved by increasing welding speed which in turn reduced the HAZ-softening. In addition, it was also reported that changes in the microstructure and hardness in the HAZ and FZ, in diode laser welds with similar and dissimilar combination of DP600 and DP980 steel, resulted in a change of fatigue performance [13,14].

The important outcome of the above mentioned studies was that microstructural heterogeneity (mainly HAZ-softening) significantly affects the mechanical properties such as tensile and fatigue strength and also the formability of laser welded HSLA and DP980 joints. High speed fiber laser welding (FLW) is becoming increasingly important and its share in the total laser industry is expected to grow substantially [8]. One of the reasons is that the high power density, small beam divergence and focal spot diameter could lead to welds with a higher penetration and smaller width for a given welding speed [7]. However, there is no report so far on the effect of FLW on the microstructure and mechanical properties of the

* Corresponding author. Tel.: +1 416 979 5000x6487; fax: +1 416 979 5265.
E-mail address: dchen@ryerson.ca (D.L. Chen).

0261-3069/$ - see front matter © 2012 Elsevier Ltd. All rights reserved.
http://dx.doi.org/10.1016/j.matdes.2012.07.017

Table 1
Compositions of the HSLA and DP980 steel used in the present study.

Steel grade	C	Mn	Si	Al	Mo	Cr	N
HSLA	0.0795	0.827	0.454	0.048	0.007	0.033	0.007
DP980	0.15	1.5	0.31	0.05	N/A	N/A	N/A

important automotive steels namely HSLA and DP980. It is unclear how serious the HAZ softening in the HSLA and DP980 steels after FLW is, and if the multiple linear FLW would have a significant effect on the fatigue strength. This study was, therefore, aimed at identifying the evolution of microstructure and the effects of FLW on the fatigue resistance in HSLA and DP980 steels. The effects of weld geometry, i.e., single and multiple linear welds, on the microstructure and fatigue properties of the welded joints have also been evaluated.

2. Material and experimental procedure

The starting materials in the present study were hot-dip galvanizing (GI) coated HSLA and DP980 steel with a thickness of 1.2 mm; the chemical compositions of the steels are given in Table 1. Butt welding of the steel sheets was carried out using an IPG PhotonicsYLS-6000 fiber laser system with a power of 6 kW, a welding speed of 16 m/min, a focal length of 30 cm. The fiber laser had a fiber core diameter of 0.3 mm with a laser beam spot size/diameter of 0.6 mm. The weld geometries and dimensions of the steel sheets used in this study are shown in Fig. 1a. Welding was performed with 0° head angle, i.e., the laser beam was perpendicular to the surface of work pieces and without any shielding gas. The metallographic samples for the microstructural examination were cut from the weld cross-section, then mounted, ground, polished, and etched with a 2% Nital solution. The etched samples were observed using a light microscope along with a Clemex image analysis system and JEOL JSM-6380 scanning electron microscope (SEM), equipped with Oxford energy dispersive X-ray spectroscopy (EDS) and three-dimensional fractographic analysis capacity. Vickers microhardness was measured on the polished samples across the weld using a computerized microhardness tester at a load of 200 g and a dwell time of 15 s. All indentations were adequately spaced to prevent any potential effect of strain fields caused by adjacent indentations. To ensure the validity of test results, two calibration tests were done using a standard reference test block before the microhardness tests on the welded joints.

Tensile and fatigue test samples following ASTM-E8/E8M standard [15] were sectioned from the welded blanks in the rolling direction (i.e., perpendicular to the welding direction), the examples of which are indicated by the dashed line in Fig. 1a with the geometry and dimensions of the test coupons shown in Fig. 1b and c. The test coupons were machined in such a way that the weld was positioned at the center of gauge length for the single linear weld (Fig. 1b), or two welds were located within the gauge length symmetrically with respect to the middle of the sample (Fig. 1c). To identify the effect of welding and its geometry on the tensile and fatigue properties, coupons of the BM were also prepared and tested. Tensile tests were conducted using a fully computerized United tensile testing machine at room temperature and with a range of strain rates from 1×10^{-5} to 1×10^{-2} s^{-1}. An extensometer with a gauge length of 50 mm and a strain limit of 20% was used to measure the strain during the tensile tests. Load control fatigue tests were performed in accordance with ASTM E466 [16] on a fully computerized Instron 8801 servo-hydraulic testing system. To avoid potential buckling of the test specimens, tension–tension cyclic loading at a stress ratio of $R = 0.1$ was applied at a frequency

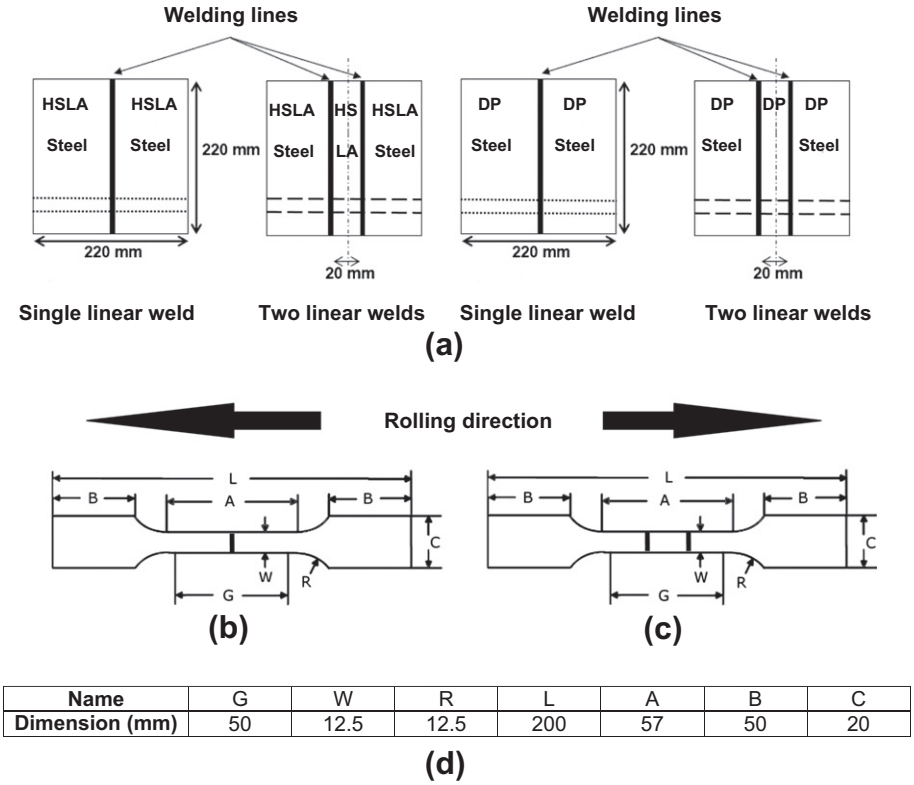

Fig. 1. Geometry and dimensions of work pieces and test specimens, (a) work pieces to be welded using a 6 kW fiber laser, (b) tensile and fatigue test samples sectioned from the single linear weld indicated by the short-dashed lines at (a), (c) tensile and fatigue test samples cut from the multiple linear weld indicated by the long-dashed lines at (a), and (d) a table of the specimen dimensions.

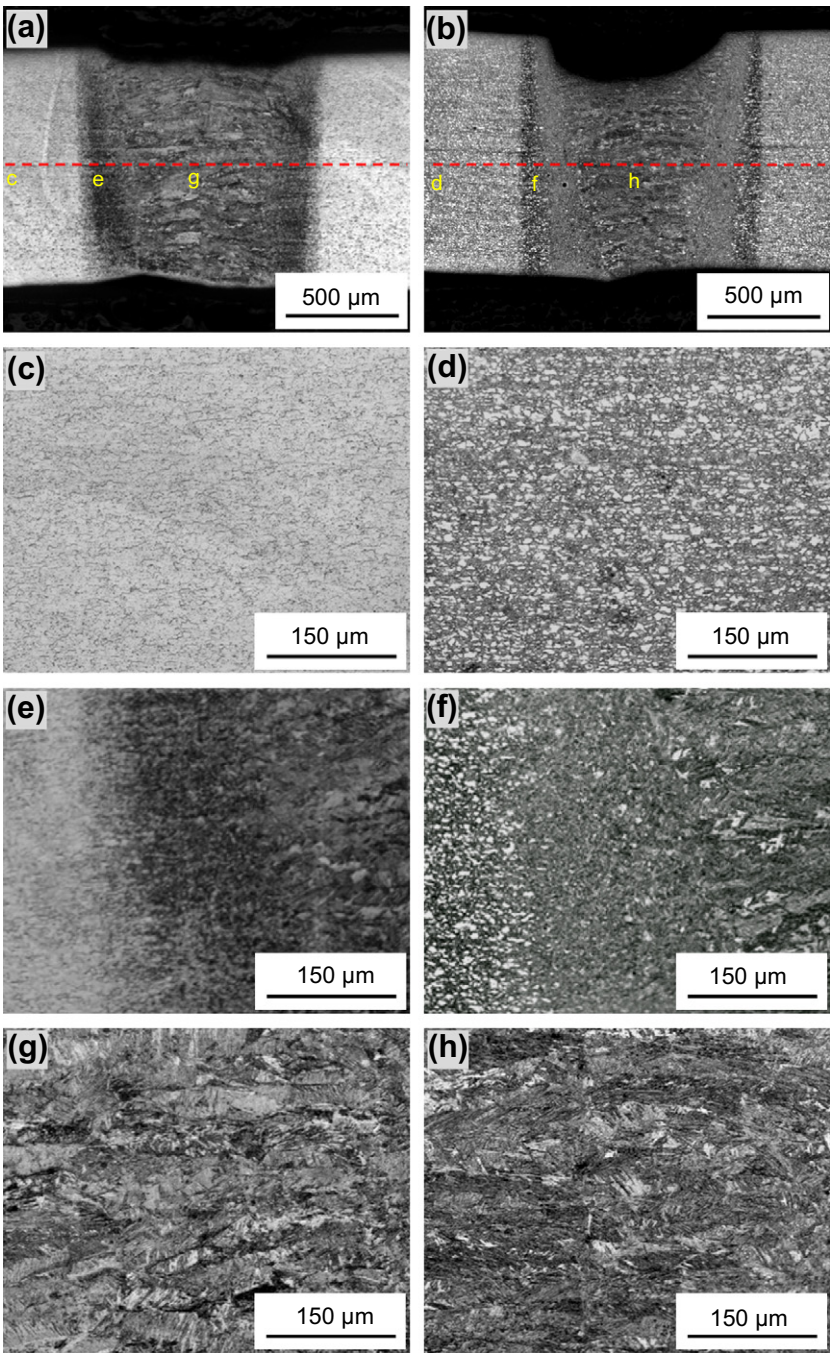

Fig. 2. Micrographs showing the microstructure change of a FLW HSLA and a FLW DP980 steel joint, (a) overall view of the cross section of the FLW HSLA steel joint, (b) overall view of the cross section of the FLW DP980 steel joint, (c) HSLA BM, (d) DP980 BM, (e) HAZ of the FLW HSLA steel joint, (f) HAZ of the FLW DP980 steel joint, (g) FZ of the FLW HSLA steel joint and (h) FZ of the FLW DP980 steel joint.

Table 2
Comparison of the average width of HAZ and FZ in the welded joints made with different types of laser welding.

Welding type	Power (kW)	Welding speed (m/min)	Spot size (mm)	Welding materials	Thickness of workpiece (mm)	Average width of HAZ (μm)	Average width of FZ (μm)	Reference
DLW	4	1.6	$12 * 0.5$	DP980 steel	1.2	4000	3000	[11]
Nd:YAG Laser welding	3	3	0.6	DP980 steel	1.17	1000	750	[10]
CO_2 laser welding	6	6	–	DP780 steel	1.8	1000	1000	[12]
FLW	6	16	0.6	DP980 steel	1.2	250	450	Present study

of 50 Hz and sinusoidal waveform. In both tensile and fatigue tests, at least two specimens were tested at each strain rate or each cyclic stress amplitude. The fatigue fracture surfaces were examined via a scanning electron microscope (SEM) to identify the initiation sites and propagation mechanism of the fatigue crack.

3. Results and discussion

3.1. Microstructure evolution

The representative weld cross-section profiles and microstructure at different weld zones of the HSLA and DP980 joints made with the FLW are shown in Fig. 2. The cross-section of the welds showed a significant microstructural change in both HSLA and DP980 joints, indicating the formation of the middle FZ and two adjacent HAZs which coexisted with the unaffected BM at both left and right ends as indicated in Fig. 2a and b. It is seen that the width of HAZ and FZ in both HSLA and DP980 joints was similar with an average of 200–300 μm, and 400–500 μm, respectively. The HAZ and FZ were narrower when compared to those formed in other laser welding (Table 2). For instance, a 4 kW DLW of 1.2 mm thick DP980 steel sheets resulted in 4 mm wide HAZ and 3 mm wide FZ [11]. This was attributed to considerably larger laser beam size (6 mm^2 for the DLW versus 0.28 mm^2 for the FLW), where the lower energy density (less than 10^6 W/cm^2) produced conduction mode. In contrast, in the FLW process the higher energy density which caused keyhole mode made welding more efficient compared with DLW [10,17,18], and the FLW could be operated at higher welding speed with a narrower weld (Table 2).

HSLA BM consisted of fine grained ferrite matrix with a uniform dispersion of fine alloy carbides (Fig. 2c), whereas martensite phase embedded in a continuous ferrite matrix was seen in DP980 BM (Fig. 2d). The volume fraction of martensite in the DP980 BM was estimated to be ~56% using image analysis in SEM, which matched closely with the earlier studies on the DP980 steel of similar chemistry [13,19–21]. Fig. 2e and f showed the microstructural changes of HAZ in both HSLA and DP980 joints, where the typical micrographs were taken from the HAZ positioned at the left side of FZ corresponding to "e" in Fig. 2a and "f" in Fig. 2b. The details of HAZ microstructure will be discussed in the later section. The microstructure in the FZ depended heavily on the heat input and cooling rate. Based on a continuous-cooling transformation (CCT) diagram of weld metal of low carbon steel, the FZ microstructure would contain a combination of grain boundary ferrite, side-plate ferrite, accicular ferrite, bainite and martensite [22]. However, Fig. 2g and h clearly showed that fully martensitic structure formed in the FZ of both HSLA and DP980 joints after the present FLW. The reason for this, based on the CCT diagram of weld metal of low carbon steel [22], was believed to be associated with the much higher power density and rapid cooling rate in the FZ during FLW, where the cooling curve being steeper enough missed to touch the nose of the *C*-curves, thus resulting in only martensite transformation. Sreenivasan et al. [10] reported a similar result for a 3 kW Nd:YAG laser welding applied on the DP980 steel sheets with a thickness of 1.17 mm. It should be noted that similar microstructural change was observed in the case of the multiple linear welds except the presence of twice microstructural heterogeneities, i.e., FZ and HAZ, because of doubling the linear welds. Thus, their microstructure was not presented here.

SEM images of the inter-critical HAZ (experiencing temperatures between Ac_1 and Ac_3 lines) with adjacent BM and upper-critical HAZ (region above Ac_3 line) of HSLA joint are shown in Fig. 3. The HSLA BM microstructure (Fig. 3b was confirmed to consist of ferrite grains with finely dispersed alloy carbide particles as observed in optical image (Fig. 2c). Fig. 3c represented the microstructure containing some martensite which formed as a product of fast cooling from the inter-critical region, where the partially formed austenite (i.e., co-existence of ferrite and austenite) transformed to martensite during fast cooling down to room temperature in the FLW process. However, it should be pointed out that the HAZ of HSLA joint did not involve any microstructural changes at the sub-critical region (below Ac_1 line) due to the absence of martensite in its BM.

On the other hand, for DP980 steel after FLW a tempered martensite area (or sub-critical region below Ac_1 line) located in-between the BM and inter-critical zone (between Ac_1 and Ac_3

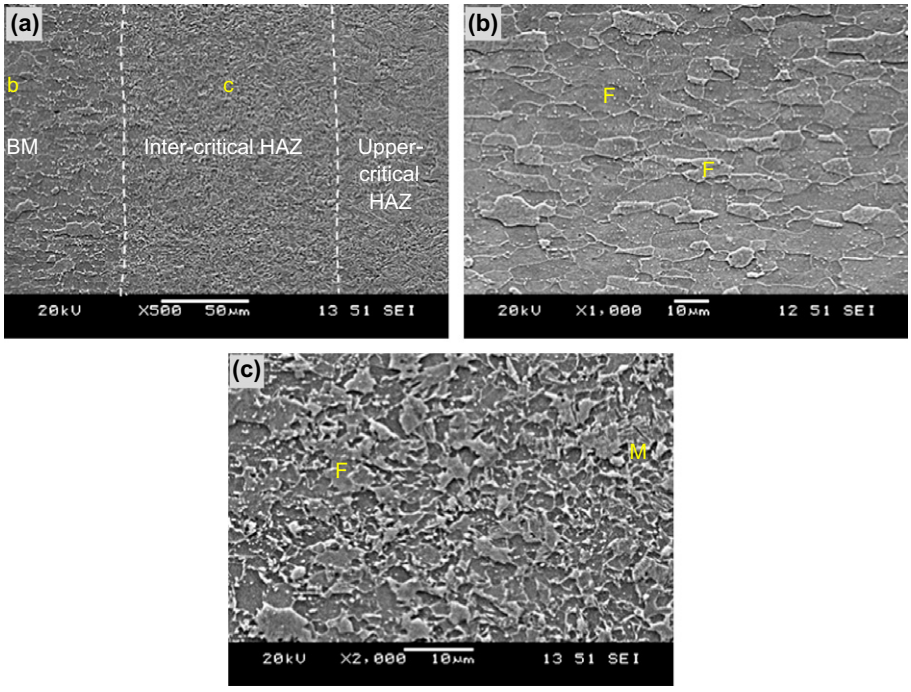

Fig. 3. SEM micrographs showing the HAZ microstructure change in the FLW of HSLA steel, (a) overall view of inter-critical HAZ with adjacent BM and upper-critical HAZ, (b) HSLA BM with ferrite and fine alloy carbides, and (c) inter-critical HAZ showing newly formed martensite phase (M: martensite, and F: ferrite).

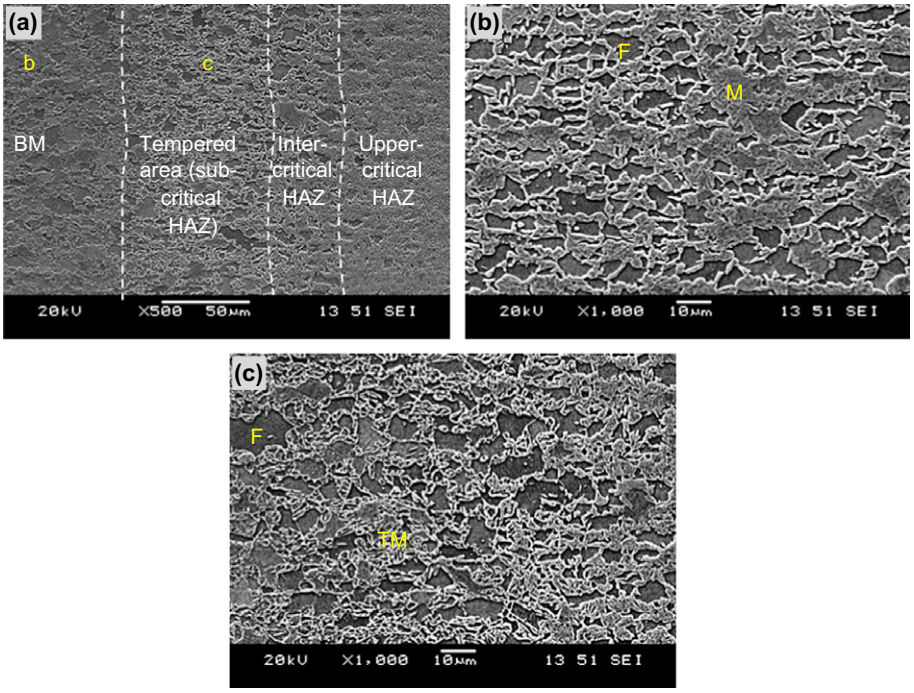

Fig. 4. SEM micrographs showing the microstructural change in a DP980 steel joint, (a) overall view of tempered martensite area in the HAZ with adjacent BM, inter-critical HAZ, and upper-critical HAZ, (b) DP980 BM showing ferrite and martensite, and (c) tempered martensite region in the HAZ (M: martensite, TM: tempered martensite, and F: ferrite).

lines), along with an upper-critical HAZ (above Ac_3 line) could be seen in Fig. 4a. While the microstructure in the inter-critical zone was somewhat similar to that in the BM with ferrite plus martensite islands, in the tempered martensite area some extent of decomposition of the martensite pre-existed in the BM (Fig. 4b) was clearly visible at a higher magnification as shown in Fig. 4c. Tempered martensite and the resultant softening zone in the laser welding of DP980 steel have been reported in many earlier studies [11,13,14,23]. In general, the temperature undergone in the softening region during welding was close to or below the critical temperature (Ac_1 at which austenite begins to form during heating) which led to high temperature tempering of martensite phase in the BM of DP steels [11,13,14,20,23–25]. The microstructure of tempered martensite in DP980 welds has been reported to consist typically of uniformly distributed fine precipitated cementite (Fe_3C) particles embedded within a continuous ferrite matrix [20,26–28]. As seen from Fig. 4c, it was clear that only partial tempering of martensite occurred in the HAZ of DP980 in the FLW process.

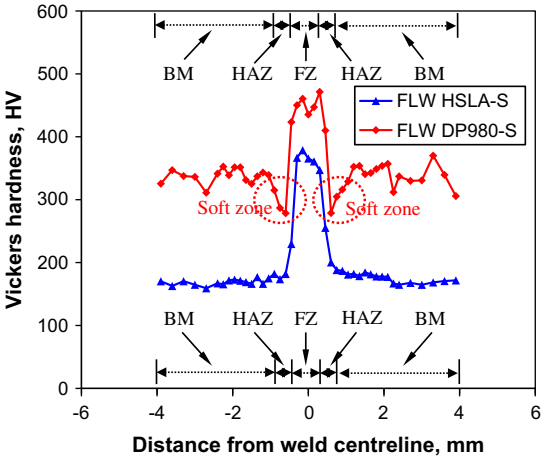

Fig. 5. Representative hardness profiles across the HSLA-S and DP980-S joints.

3.2. Hardness profiles

Vickers microhardness profiles across the welds of the FLW HSLA single linear joint (FLW HSLA-S) and the FLW DP980 single linear joint (FLW DP980-S) (as indicated by the red[1] dashed lines in Fig 2a and b) are showed in Fig. 5. The average hardness value of the HSLA and DP980 steel BM was measured to be about 170 HV and 340 HV, respectively. The higher hardness in the DP980 BM was attributed to the presence of higher fraction of hard martensite phase (~56%, Fig. 2d and Fig. 4b), while the HSLA BM did not contain any martensite (Fig. 2c and Fig. 3b). In accordance with the microstructure (Fig. 2g and h) where fully martensitic structure emerged, the hardness of the FZ became much higher and showed a decrease from FZ to the HAZ. Interestingly, the hardness curve though the whole HAZ was seen to merge smoothly into the unaffected BM in the HSLA joint due to a decrease in the fraction of martensite in the HAZ which formed as a solid-state phase transformation from austenite in the inter-critical region. On the other hand, the hardness pattern in the DP980 joint exhibited two soft zone "valleys" beside the center FZ, where the hardness locally dropped significantly to an average of 280 HV which was well below the DP980 BM hardness (~350 HV). This was attributed to the occurrence of martensite tempering (HAZ-softened region) as discussed above and also illustrated in Fig. 4. The narrow FZ with fully martensitic microstructure in both HSLA and DP980 joints after FLW were characterized by a very high hardness (Fig. 5). However, the DP980 joint had a further higher hardness averaging 450 HV compared with the average FZ hardness (360 HV) in the HSLA joint. This was mainly due to the fact that

[1] For interpretation of color in Figs. 2-11, the reader is referred to the web version of this article.

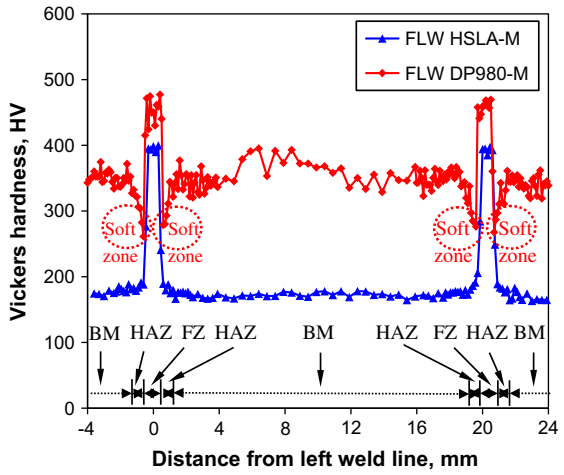

Fig. 6. Typical hardness profiles across the HSLA-M and DP980-M joints.

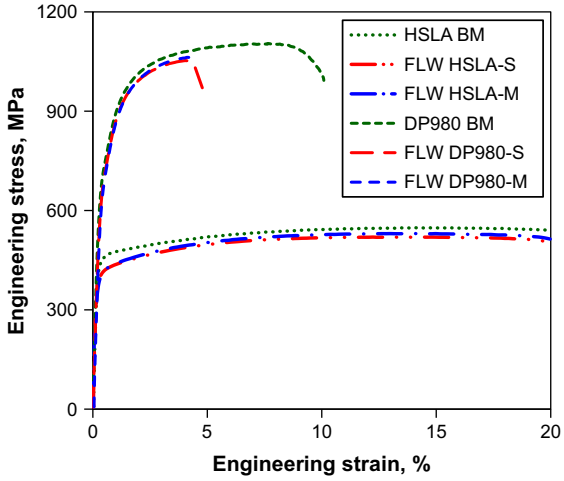

Fig. 7. Representative engineering stress versus engineering strain curves of HSLA BM, FLW HSLA-S joint, FLW HSLA-M joint, DP980 BM, FLW DP980-S joint, FLW DP980-M joint tested at a strain rate of $1 \times 10^{-3}\ s^{-1}$.

the martensite in the FZ of DP980 joint contained a higher amount of carbon, as seen in Table 1 where nearly twice carbon content was present in the DP980 steel compared with the HSLA steel. Additionally, nearly doubled manganese content in the DP980 steel (Table 1) also contributed to the higher hardness [29]. Calcagnotto et al. [30] noted that Mn was able to increase hardneability substantially just like carbon content in austenite on grain size stability and hardneability in ultrafine-grained ferrite/martensite dual-phase steel.

Fig. 6 shows the microhardness profiles across the multiple linear weld of FLW HSLA (FLW HSLA-M) and FLW DP980 (FLW DP980-M) joints. Both FLW HSLA-M and FLW DP980-M joints were observed to display a "suspension bridge"-like or "cable-stayed bridge"-like hardness profile with two FZ hardness representing the "pylons or towers". It is seen that each weld bead of the multiple linear joints (Fig. 6) had a similar hardness values when compared it to the single linear joints (Fig. 5), which was a result of similar microstructures as noted in the previous section. The distinction between the FLW HSLA-M and FLW DP980-M joints was that the hardness profile of the former was smoother without "valleys" due to the absence of HAZ-softening (martensite tempering). On the contrary, in the FLW DP980-M joint each FZ hardness "pylon" was accompanied by two soft zone "valleys" positioned at its two sides (Fig. 6). It would be of interest to see if doubling the number of soft zones would affect tensile strength and fatigue life of the HSLA and DP980 joints.

3.3. Tensile properties

The representative engineering stress versus engineering strain curves, determined at a strain rate of $1 \times 10^{-3}\ s^{-1}$, of the BM, FLW single and multiple linear joints of both HSLA and DP980 steels are illustrated in Fig. 7. In the HSLA joints, both the strain to failure and the yield strength (YS) after welding were observed to be very close to those of the BM. The evaluated tensile test results are listed in Table 3. The YS and ultimate tensile strength (UTS) were obtained to be 400 MPa and 515 MPa, respectively, for the FLW HSLA-S joint and 398 MPa and 523 MPa, respectively, for the FLW HSLA-M joint. These values were fairly close to those of the BM which had a YS of 455 MPa and UTS of 546 MPa (Table 3, and Fig. 7). These tensile results suggested that the present FLW process, regardless of single or multiple linear welding had little influence on the tensile properties of the HSLA steel. Obviously, this was because the FLW of HSLA steel did not create any soft zone (Fig. 5 and 6) in the HAZ that was detrimental to the mechanical properties of the welds. This was also corroborated by the tensile failure of FLW HSLA joints that consistently occurred in the BM. This finding was also in agreement with the earlier observations on the tensile failure locations by Xia et al. in a DLW HSLA joint [11], Farabi et al. [31] in a diode laser welded DP600 steel joint, and Panda et al. [32] in a diode laser welded HSLA/DP980 dissimilar joint with a thickness of 1.14 mm and 1.17 mm, respectively.

In contrast to the HSLA welds, the DP980 joints showed a lower strain to failure (Fig. 7 and Table 3). However, the YS and UTS were basically unaffected by the FLW. As seen in Table 2, the strength of FLW DP980-S joints (YS = 719 MPa; UTS = 1048 MPa) and FLW DP980-M joints (YS = 717 MPa, UTS = 1066 MPa) was very close to those of the BM (YS = 720 MPa; UTS = 1095 MPa). The results indicated that the presence of narrow soft zone in the FLW DP980 welds was not detrimental to the tensile strength, and the high welding speed could greatly reduce the harmful influence of the soft zone by narrowing it down significantly.

It was also of interest to observe that a joint efficiency (i.e., a ratio of the UTS of welded joints to the UTS of the corresponding BM [33–35]) of both FLW HSLA joints and FLW DP980 joints reached as high as about 94–96% and 96–97% (Table 3), respectively. These

Table 3
Tensile properties and fatigue parameters σ_f' and b for HSLA BM, FLW HSLA-S joint, FLW HSLA-M joint, DP980 BM, FLW DP980-S joint, and FLW DP980-M joint.

Welding type	Yield strength (MPa)	Ultimate tensile strength (MPa)	Elongation (%)	Joint efficiency (%)	Fatigue limit (MPa)	Fatigue ratio	σ_f' (MPa)	b
HSLA BM	455	546	24.7	–	200	0.366	302	−0.023
FLW HSLA-S	400	515	22.7	94.3	125	0.243	328	−0.041
FLW HSLA-M	398	523	20.7	95.8	125	0.239	343	−0.048
DP980 BM	720	1095	14.2	–	250	0.228	1019	−0.098
FLW DP980-S	719	1048	4.6	95.7	150	0.143	1169	−0.132
FLW DP980-M	717	1066	5.1	97.3	150	0.141	1984	−0.185

results were similar to those of Nd:YAG laser welding (94.1% for DP980 steel joints) [12] and CO_2 laser welding (96.9% for CP1180 steel joints [12]). Indeed, if one considers the ratio of the YS of welded joints to the YS of the corresponding BM, a nearly 100% YS joint efficiency would be achieved in both FLW DP980-S and FLW DP980-M joints. From these tensile results it can be concluded that FLW is an able and viable joining process that gave rise to superior tensile performance approaching that of BMs for both HSLA and DP980 steels, while the FLW DP980 joints had a much higher tensile strength than the FLW HSLA joints.

However, it should be noted that, while the percent elongation or ductility of both FLW HSLA-S and HSLA-M joints (~21–23%) came fairly close to that of the HSLA BM (~25%) as shown in Table 3, the ductility of the FLW DP980-S joints (4.6%) and the FLW DP980-M joints (5.1%) was noticeably lower than that of the BM (14.2%) since all the tensile test samples failed consistently in the soft zone. The lower ductility in the DP980 welds was due to the fact that yielding occurred first in one of the soft zones and the subsequent plastic deformation was predominantly concentrated there leading to necking and premature failure at that location, which resulted in a reduction in the overall specimen elongation. Similar results have also been reported in the study of formability of DLW of DP980 [11,32]. It was also due to the premature failure induced by the soft zone (i.e., lower ductility) that the UTS of FLW joints became lower (Fig. 7), although a high joint efficiency of about 96–97% was achieved in the FLW DP980 joints.

3.4. Fatigue strength and failure mode

Fatigue test results of the BM, FLW single linear and multiple linear joints of HSLA tested at $R = 0.1$, 50 Hz, and room temperature (RT) are plotted in the Fig. 8a. Both FLW HSLA-S and HSLA-M joints exhibited an equivalent fatigue life within the experimental scatter. At a stress amplitude of above 250 MPa the fatigue life of the joints was only slightly lower than that of the BM, whereas the fatigue strength became lower and more scattered at lower stress amplitudes (<250 MPa). In FLW HSLA welds, in spite of the absence of HAZ-softening (Fig. 5 and 6), welding could destroy the surface continuance, change the surface residual stress distribution, and create the weld concavity on the surface (Fig. 2a). These could promote the fatigue crack initiation and propagation, thus reducing fatigue life [34,36]. Interestingly, the multiple linear welded HSLA samples exhibited an equivalent fatigue strength at both higher and lower levels of stress amplitudes to that of the single linear welds, indicating that the probability of dynamic fatigue failure was not affected by the weld geometry or by increasing number of welds, i.e., HAZ and FZ in the HSLA.

The *S–N* curves of DP980 BM, FLW DP980-S joints, and FLW DP980-M joints tested at $R = 0.1$, 50 Hz, and RT are shown in the Fig. 8b. The FLW DP980-S joints represented an equivalent or only slightly lower fatigue life than the BM at a stress amplitude above 250 MPa, whereas the fatigue strength became lower and more scattered below a stress amplitude of 250 MPa. This indicated that while the narrow HAZ-softening (Fig. 2b, Fig. 4a, and Fig. 6) did not affect the static tensile strength (Fig. 7 and Table 2), the dynamic fatigue resistance was susceptible to the presence of the soft zone. This observation corresponded well to that reported by Roesler et al. [37] who pointed out that the fatigue strength of a material under dynamic cyclic loading was much more sensitive to the manufacturing process and materials than the static strength, and that the fatigue strength was also much more sensitive to the lower level cyclic load than the higher level cyclic load. Indeed, in the region of lower level of stress amplitude and longer life, the factors like surface conditions, residual stresses, localized stress concentration, surface protective coating, severe weld concavity and zinc inclusions in weldment are deleterious to fatigue life [35,36]. The fatigue data plotted in Fig. 8b for the multiple linear welds exhibited a larger scatter and lower fatigue strength (e.g., two samples failed at a stress amplitude of 150 MPa), implying that the probability of dynamic fatigue failure at the lower level of

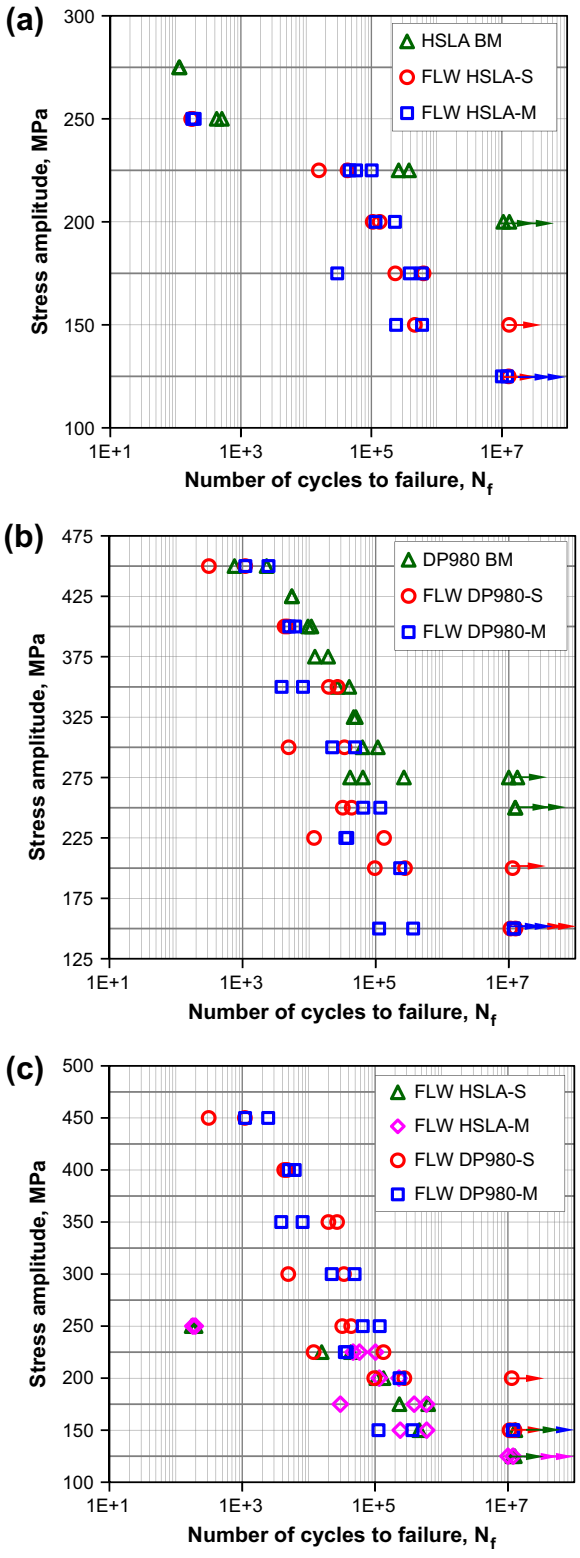

Fig. 8. *S–N* curves of (a) the HSLA BM, FLW HSLA-S joints and FLW HSLA-M joints, (b) the DP980 BM, FLW DP980-S joints and FLW DP980-M joints, and (c) FLW HSLA-S joints, FLW HSLA-M joints, FLW DP980-S joints and FLW DP980-M joint tested at $R = 0.1$, 50 Hz, and RT.

stress amplitudes increased with increasing number of soft zones in the higher grade of DP980.

To make a better comparison, fatigue test results of the FLW HSLA-S joints, the FLW HSLA-M joints, the FLW DP980-S joints, and the FLW DP980-M joints were plotted in Fig. 8c. The FLW DP980 joints were observed to have a much higher fatigue strength than that of the FLW HSLA joints at a stress amplitude above 250 MPa, but the fatigue strength was equivalent below a stress amplitude of 250 MPa for both DP980 and HSLA joints due to the fact that the higher grade/strength of DP980 was more sensitive to the presence of severe weld concavity (Fig. 2b) especially at the lower level of cyclic load than at the higher level of cyclic load.

Fatigue limit and fatigue ratio are tabulated in Table 3. The decrease in fatigue limit for both FLW HSLA and FLW DP980 joints, with respect to their BM, were similar at 37.5% and 40%, respectively, while the fatigue limit of the FLW DP980 joints were 20% higher than that of the FLW HSLA joints. The fatigue ratio (i.e., a ratio of fatigue limit to the UTS) of the FLW HSLA-S joints and the FLW DP980-S joints were 0.243 and 0.143, respectively. The lower fatigue ratio of FLW DP980-S joints was related to its much higher (or twice) UTS (Table 3). These results suggested that while the tensile strength of the FLW DP980 joints was much higher than that of the FLW HSLA joints, the fatigue strength was very close for both joints at a lower level of stress amplitudes (<250 MPa). Another factor for the lower fatigue limit or fatigue ratio in both types of FLW joints was associated with the notch effect of weld concavity, since fatigue is a type of notch-sensitive dynamic failure. As seen in Fig. 2a and b, the FLW "notch" or weld concavity

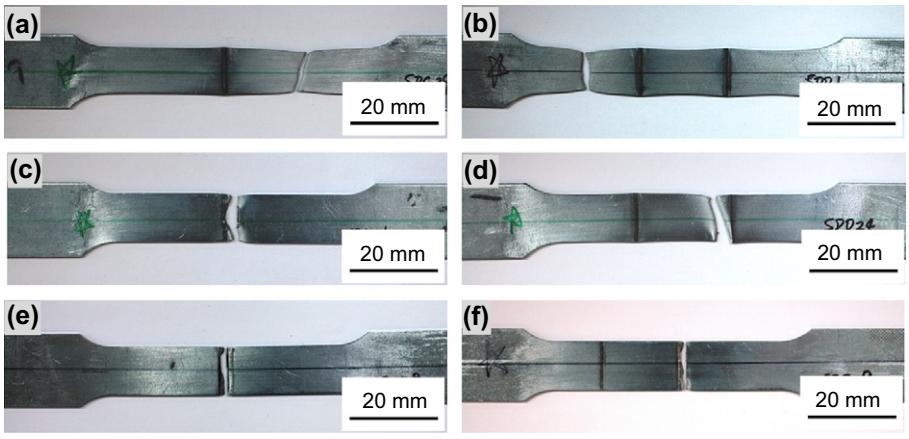

Fig. 9. Typical fatigue failure locations of (a) a HSLA-S joint at a stress amplitude above 250 MPa, (b) a HSLA-M joint at a stress amplitude above 250 MPa, (c) a HSLA-S joint below stress amplitude of 250 MPa, (d) a HSLA-M joint below stress amplitude of 250 MPa, (e) a DP980-S joint, and (f) a DP980-M joint.

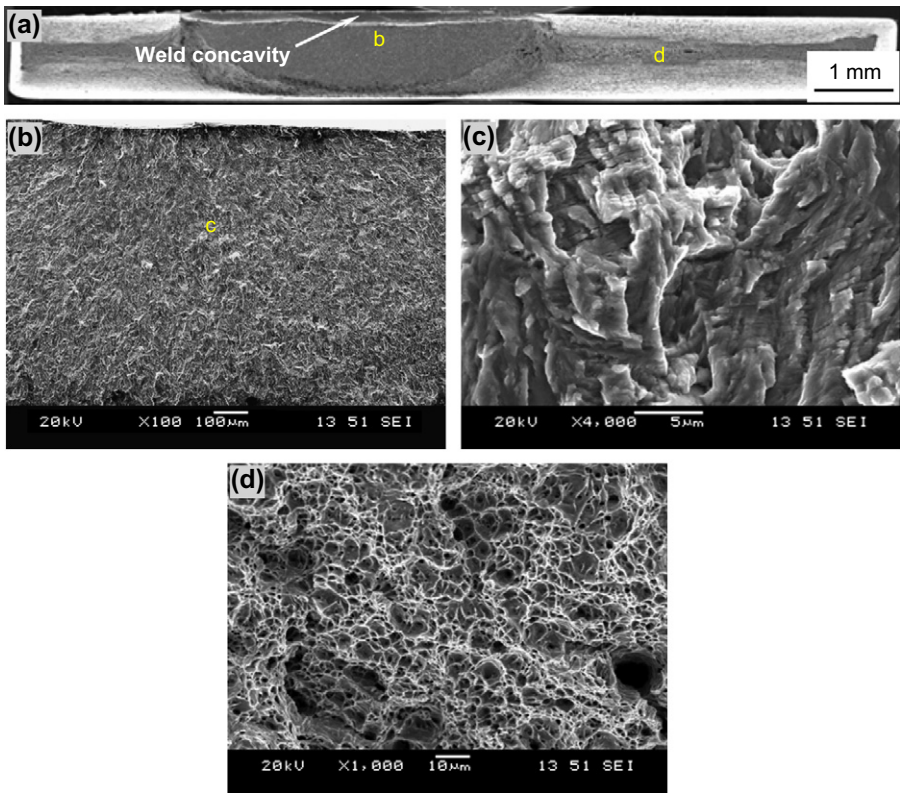

Fig. 10. Typical SEM images of fatigue fracture surface of a FLW HSLA-S joint tested at a stress amplitude 200 MPa, (a) overall view, (b) crack initiation area, (c) crack propagation area, and (d) final fast crack propagation area.

in both joints was similar to a notched specimen studied by Chapetti et al. [38] where the stress concentration was generated, and consequently a decreased fatigue limit or fatigue life at the low level of stress amplitudes was observed. Further studies are needed to eliminate the weld concavity and improve the fatigue resistance.

The obtained fatigue data plotted in Fig. 8 could be fitted using the following Basquin type equation,

$$\sigma_a = \sigma'_f(2N)^b \quad (1)$$

where σ_a is the stress amplitude, σ'_f is the fatigue strength coefficient defined by the stress intercept at $2N = 1$, N is the number of cycle to failure, and b is the fatigue strength exponent. The obtained values of σ'_f and b of the BM, the FLW single linear joint and the FLW multiple linear joints for both HSLA and DP980 steels tested at $R = 0.1$, 50 Hz and room temperature are given in Table 3. Apparently, the fatigue life at a given stress amplitude was dependent on both fatigue strength coefficient σ'_f and fatigue strength exponent b with b being a predominant factor. The smaller the absolute value of b, the longer the fatigue life. It is seen from Table 3 that after FSW for both HSLA and DP980 steels the absolute values of b became larger, giving rise to a lower fatigue life after welding.

3.5. Failure location and fractography

The typical fatigue failure locations for the HSLA-S joints, the HSLA-M joints, the DP980-S joints and the DP980-M joints are shown in Fig. 9. It is seen that the fatigue failure for the FLW HSLA joints occurred in the BM with large deformation at a stress amplitude above 250 MPa (Fig. 9a and b), whereas it occurred at HAZ below a stress amplitude of 250 MPa (Fig. 9c and d), irrespective of the single or multiple linear welding. It was believed that while the weld concavity in the FLW HSLA joints (Fig. 2a) did not significantly influence the tensile strength (Fig. 7 and Table 3), the fatigue strength at the condition of stress amplitude below 250 MPa was affected adversely. In contrast, the fatigue failure in the FLW DP980 joints always initiated in weld concavity (Fig. 9e and f) due to the presence of stress concentration, and then propagated in the soft zone (Fig. 5 and 6). The failure location of the FLW joints was similar to that of the DLW DP980 joints in which all the fatigue failure occurred at the soft zones as reported in our earlier study [39].

SEM images of a fracture surface of a FLW HSLA-S joint tested at an applied stress amplitude of 200 MPa is shown in Fig. 10. The cross section in Fig 10a indicated that the fatigue test sample experienced a large deformation before the final fast crack propagation because of the superior ductility of HSLA steel in comparison with DP980 steel (Table 3). It was also confirmed from Fig. 10a and b that crack initiation occurred from the weld concavity (Fig. 2a), corresponding well to the top view of the failed samples (Fig. 9c and d). A magnified SEM image near the crack initiation site is shown in Fig. 10b, where the crack initiated from the weld concavity could clearly be seen when the applied stress amplitude was below 250 MPa. Fatigue crack propagation was mainly characterized by the formation of fairly typical fatigue striations in conjunction with secondary cracks, as shown in Fig. 10c, while the final fast propagation area consisted of distinctive dimples (Fig. 10d). Fatigue striations basically occurred through a repeated plastic blunting–sharpening process via the slip of dislocations in the plastic zone in front of the fatigue crack tip [40].

SEM images of a fracture surface of a FLW DP980-S joint tested at an applied stress amplitude of 200 MPa is shown in Fig. 11. It is from Fig. 11a that multiple crack initiation occurred from the weld concavity where the surface welding defect occurs (Fig. 11b) as indicated by the arrow in the image. These characteristics of the

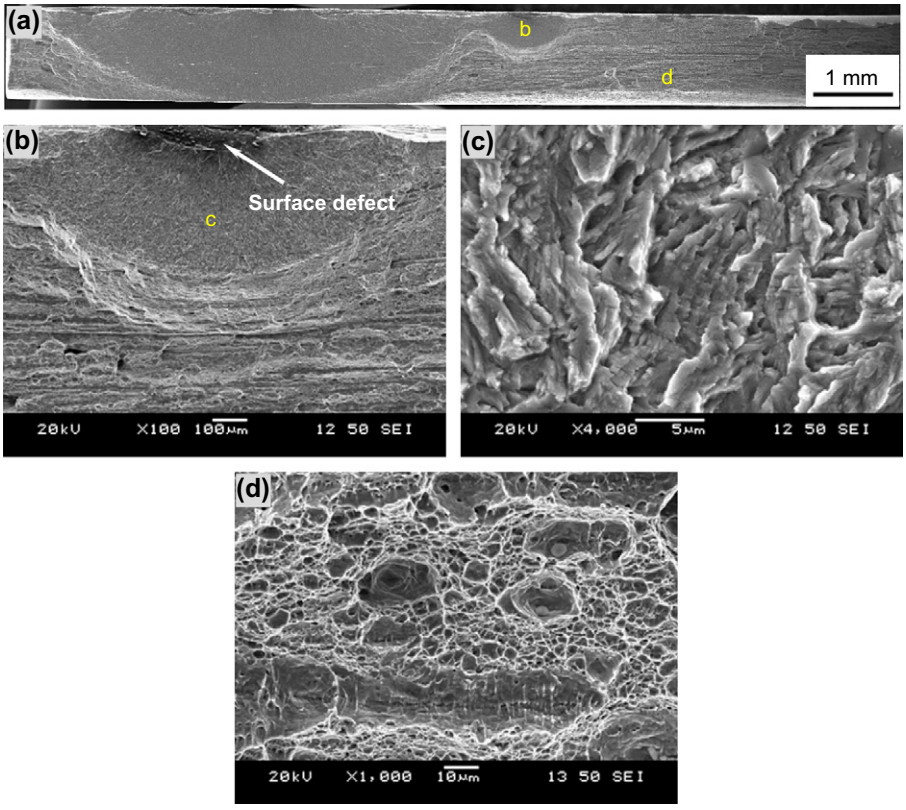

Fig. 11. Typical SEM images of fatigue fracture surface of a FLW DP980-S joint tested at a stress amplitude 200 MPa, (a) overall view, (b) crack initiation area, (c) crack propagation area, and (d) final fast crack propagation area.

fatigue fractograph were similar to those observed on the fatigue fracture surface reported for a FLW AZ31B-H24 Mg alloy [35]. The fatigue crack initiation in the present FLW DP980 steel would primarily be related to the stress concentration caused by the severe weld concavity (Fig. 2b), in combination with the presence of detrimental soft zones (Fig. 5 and 6). Like the HSLA welds, fatigue crack propagation in the FLW DP980 joints was also characterized by the occurrence of fatigue striations along with secondary cracks, as shown in Fig. 11c, whereas the final fast propagation area consisted of characteristic dimples as well, as shown in Fig. 11d, where some remaining inclusions located at the bottom of dimples could be seen.

4. Conclusions

In this study the microstructure, hardness profile, tensile properties, and fatigue performance of high speed fiber laser welded HSLA and DP980 steel joints with single linear and multiple linear welds are evaluated and compared. The following conclusions can be drawn:

(1) Single phase microstructure containing martensite formed in the FZ of all the joints; however, newly formed martensite and partially tempered martensite structure was observed in the (HAZ) of HSLA and DP980 steels, respectively.
(2) The HSLA joints exhibited a hardness profile with HAZ hardness merging smoothly into the unaffected BM values, while the DP980 joints showed a significant drop of hardness in the HAZ. Despite the formation of fully martensitic structure in the FZ, the higher carbon content in DP980 steel resulted in a higher FZ hardness (~450 HV) compared to HSLA steel (~360 HV). A characteristic "suspension bridge"-like hardness profile with the FZ hardness as a "pylon" was observed.
(3) Both the HSLA and DP980 joints showed a superior tensile strength with a joint efficiency reaching about 94–97%. While the ductility of DP980 joints decreased, the ductility of HSLA joints was fairly close to that of BM. Despite the presence of the soft zone, the ultimate tensile strength of the DP980 joints was twice higher than that of the HSLA joints, which corresponded well to the hardness results.
(4) The DP980 joints had a much longer fatigue life compared to the HSLA joints at a stress amplitude above 250 MPa; however, below this stress amplitude both the DP980 and HSLA joints showed a similar fatigue life.
(5) No significant effect of weld geometry on the fatigue life of HSLA joints was observed. On the other hand, the fatigue life for the multiple linear DP980 joints exhibited a larger scatter and also lower fatigue strength, indicating that the probability of dynamic fatigue failure at the lower level of stress amplitudes increased with increasing number of soft zone and weld concavity in the weld.
(6) Above a stress amplitude of 250 MPa, fatigue failure of the HSLA joints occurred in the BM, signifying a superior structural integrity of the fiber laser welded HSLA joints when subjected to higher levels of cyclic loading. When the applied stress amplitude was below 250 MPa, fatigue failure occurred from the weld concavity.
(7) In the DP980 joints under both higher and lower levels of cyclic loading, fatigue crack was observed to initiate predominantly from the weld concavity and propagate in the soft zone. Fatigue crack propagation in both HSLA and DP980 joints was characterized by the characteristic fatigue striations coupled with secondary cracks.

Acknowledgements

The authors would like to thank the Natural Sciences and Engineering Research Council of Canada (NSERC) and AUTO21 Network of Centers of Excellence for providing financial support. The financial support from International Zinc Association (IZA) and ArcelorMittal Dofasco is highly acknowledged. One of the authors (D.L. Chen) is grateful for the financial support by the Premier's Research Excellence Award (PREA), NSERC-Discovery Accelerator Supplement (DAS) Award, Canada Foundation for Innovation (CFI), and Ryerson Research Chair (RRC) program. The authors would like to thank Dr. J. Chen and Dr. Y.L. He (CANMET-Materials Technology Laboratory, Natural Resources Canada, Hamilton, Canada), Mr. E. Biro (ArcelorMittal Global Research, Hamilton, Canada), and Dr. J. Villafuerte (CenterLine (Windsor) Ltd., Windsor, Canada) for their support and helpful discussion. The assistance of Q. Li, A. Machin, J. Amankrah, and R. Churaman in performing the experiments is gratefully acknowledged.

References

[1] Howey DA. Policy: a challenging future for cars. Nat Clim Change 2012;2:28–9.
[2] Shindell D, Faluvegi G, Walsh M, Anenberg SC, Dingenen RV, Muller NZ, et al. Climate, health, agricultural and economic impacts of tighter vehicle-emission standards. Nat Clim Change 2011;1:59–66.
[3] Kim HJ, McMillan C, Keoleian GA, Skerlos SJ. Greenhouse gas emissions payback for lightweighted vehicles using aluminum and high-strength steel. J Ind Ecol 2010;14(6):929–46.
[4] Hazratinezhad M, Arab NBM, Sufizadeh AR, Torkamany MJ. Mechanical and metallurgical properties of pulsed neodymium-doped yttrium aluminum garnet laser welding of dual phase steels. Mater Des 2012;33:83–7.
[5] Ahmed E, Reisgen U, Schleser M, Mokrov O. On formability of tailor laser welded blanks of DP/TRIP steel sheets. Sci Technol Weld Joint 2010;15:337–42.
[6] Chan LC, Cheng CH, Chan SM, Lee TC, Chow CL. Formability analysis of tailor-welded blanks of different thickness ratios. J Manuf Sci E – T ASME 2005;127:743–51.
[7] Quintino L, Costa A, Miranda R, Yapp D, Kumar V, Kong CJ. Welding with high power fiber lasers – a preliminary study. Mater Des 2007;28:1231–7.
[8] Canning J. Fiber lasers and related technologies. Opt Laser Eng 2006;44:647–76.
[9] Saunders FI, Wagoner RH. Forming of tailor-welded blanks. Metall Mater Trans A 1996;27A:2605–16.
[10] Sreenivasan N, Xia M, Lawson S, Zhou Y. Effect of laser welding on formability of DP980 steel. J Eng Mater T 2008;130:0410041–410049.
[11] Xia M, Sreenivasan N, Lawson S, Zhou Y, Tian Z. A comparative study of formability of diode laser welds in DP980 and HSLA steels. J Eng Mater Technol T A 2007;129:446–52.
[12] Kim CH, Choi JK, Kang MJ, Park YD. A study on the CO_2 laser welding characteristics of high strength steel up to 1500 MPa for automotive application. J Achiev Mater Manuf Eng 2010;39:79–86.
[13] Farabi N, Chen DL, Zhou Y. Microstructure and mechanical properties of laser welded dissimilar DP600/DP980 dual-phase steel joints. J Alloy Compd 2011;509:982–9.
[14] Farabi N, Chen DL, Zhou Y. Fatigue properties of laser welded dual-phase steel joints. Procedia Eng 2010;2:835–43.
[15] ASTM E8/E8M-11. Standard test methods for tension testing of metallic materials. ASTM international; 2012.
[16] ASTM E466–07. Standard practice for conducting force controlled constant amplitude axial fatigue tests of metallic materials. ASTM international; 2012.
[17] Duley WW. Laser welding. New York: Wiley & Sons, Inc; 1999.
[18] Ready JF, Farson DF. LIA Handbook of laser materials processing. Laser Institute of America; 2001.
[19] Xia MS, Kuntz ML, Tian ZL, Zhou Y. Failure study on laser welds of dual phase steel in formability testing. Sci Technol Weld Joint 2008;13(4):378–87.
[20] Baltazar Hernandez VH, Nayak SS, Zhou Y. Tempering of martensite in dual-phase steels and its effects on softening behavior. Metall Mater Trans A 2011;42A:3115–29.
[21] Huang T, Sato YS, Kokawa H, Miles MP, Kohkonen K, Siemssen B, et al. Microstructural evolution of DP980 steel during friction bit joining. Metall Mater Trans A 2009;40A:2994–3000.
[22] Kou S. Welding metallurgy. 2nd ed. Hoboken, NJ: John Wiley & Sons Inc; 2003.
[23] Farabi N, Chen DL, Zhou Y. Tensile properties and work hardening behavior of laser welded dual-phase steel joints. J Mater Eng Perform 2012;21(2):222–30.
[24] Xia M, Biro E, Tian ZL, Zhou Y. Effects of heat input and martensite on HAZ softening in laser welding of dual phase steels. ISIJ Int 2008;48(6):809–14.
[25] Biro E, McDermid JR, Embury JD, Zhou Y. Softening kinetics in the subcritical heat-affected zone of dual-phase steel welds. Metall Mater Trans A 2010;41(9):2348–56.

[26] Kuang S, Kang YL, Yu H, Liu RD. Effect of continuous annealing parameters on the mechanical properties and microstructures of a cold rolled dual phase steel. Int J Min Met Mater 2009;16(2):159–64.
[27] Dancette S, Massardier-Jourdan V, Fabregue D, Merlin J, Dupuy T, Bouzekri M. HAZ microstructures and local mechanical properties of high strength steels resistance spot welds. ISIJ Int 2011;51(1):99–107.
[28] Waterschoot T, Verbeken K, De Cooman BC. Tempering kinetics of the martensitic phase in DP steel. ISIJ Int 2006;46(1):138–46.
[29] Grange RA. Estimating the hardneability of carbon steels. Metall Trans 1973;4:2231–44.
[30] Calcagnotto M, Ponge D, Raabe D. On the effect of manganese on grain size stability and hardneability in ultrafine-grained ferrite/martensite dual-phase steels. Metall Mater Trans A 2012;43:37–46.
[31] Farabi N, Chen DL, Li J, Zhou Y, Dong SJ. Microstructure and mechanical properties of laser welded DP600 steel joints. Mater Sci Eng A 2010;527:1215–22.
[32] Panda SK, Baltazar Hernandez VH, Kuntz ML, Zhou Y. Formability analysis of diode-laser-welded tailored blanks of advanced high-strength steel sheets. Metall Mater Trans A 2009;40A:1955–67.
[33] Chowdhury SM, Chen DL, Bhole SD, Powidajko E, Weckman DC, Zhou Y. Microstructure and mechanical properties of fiber–laser welded and diode–laser-welded AZ31 magnesium alloy. Metall Mater Trans A 2011;42A: 1974–89.
[34] Chowdhury SM, Chen DL, Bhole SD, Cao X, Powidajko E, Weckman DC, et al. Tensile properties and strain hardening behavior of double-sided arc welded and friction stir welded AZ31B magnesium alloy. Mater Sci Eng A 2010;527:2951–61.
[35] Chowdhury SH, Chen DL, Bhole SD, Powidajko E, Weckman DC, Zhou Y. Fiber laser welded AZ31 magnesium alloy: effect of welding speed on microstructure and mechanical properties. Metall Mater Trans A 2012;43A:2133–47.
[36] Anand D, Chen DL, Bhole SD, Andreychuck P, Boudreau G. Fatigue behaviour of tailor (laser)-welded blanks for automotive applications. Mater Sci Eng A 2006;420:199–207.
[37] Roesler J, Harders H, Baeker M. Mechanical behavior of engineering materials: metals, ceramics, polymers, and composites. 1st ed. New York: Springer; 2007.
[38] Chapetti MD, Katsura N, Tagawa T, Miyata T. Static strengthening and fatigue blunt-notch sensitivity in low-carbon steels. Int J Fatigue 2001;23: 207–14.
[39] Khan MS, Bhole SD, Chen DL, Boudreau G, Biro E, Deventer JV. Welding behavior, microstructure and mechanical properties of dissimilar resistance spot welds between galvannealed HSLA350 and DP600 steels. Sci Technol Weld Joint 2009;14(7):616–25.
[40] Laird C. Fatigue crack propagation. West Conshohocken, PA: ASTM Spec. Tech. Publ.; 1967.